^{3}He + ^{4}He → ^{7}Be astrophysical *S* factor

T. A. D. Brown, C. Bordeanu,* K. A. Snover,† D. W. Storm, D. Melconian, A. L. Sallaska, S. K. L. Sjue, and S. Triambak

Center for Experimental Nuclear Physics and Astrophysics, University of Washington, Seattle, Washington 98195, USA

(Received 24 July 2007; published 2 November 2007)

We present precision measurements of the ^{3}He + ^{4}He → ^{7}Be reaction in the range $E_{\text{c.m.}} = 0.33$ to 1.23 MeV using a small gas cell and detection of both prompt γ rays and ^{7}Be activity. Our prompt and activity measurements are in good agreement within the experimental uncertainty of several percent. We find $S(0) = 0.595 \pm 0.018$ keV b from fits of the Kajino theory to our data. We compare our results with published measurements, and we discuss the consequences for Big Bang Nucleosynthesis and for solar neutrino flux calculations.

DOI: 10.1103/PhysRevC.76.055801 PACS number(s): 26.20.+f, 26.65.+t, 25.40.Lw, 25.55.−e

I. INTRODUCTION

The ^{3}He + ^{4}He → ^{7}Be fusion reaction is an important step in the solar p-p chain responsible for producing solar neutrinos from ^{7}Be and ^{8}B decay. Bahcall and Pinsonneault [1] identified it as the solar fusion reaction rate most in need of further study, because of its relatively large uncertainty. It is also reponsible for essentially all of the ^{7}Li produced in the Big Bang, a nuclide whose apparent primordial abundance remains a puzzle [2].

The ^{3}He + ^{4}He → ^{7}Be reaction rate has been determined previously by detecting the prompt γ rays [3–9] and by counting the ^{7}Be activity [7,10,11] (see Fig. 1). The accepted value for the zero-energy S factor for this reaction is based on a 1998 recommendation of $S(0) = 0.53 \pm 0.05$ keV b [12], where the relatively large uncertainty stems from an apparent disagreement between the results from the two methods. Since then, new activity measurements have been published by a Weizmann Institute group [13], and the LUNA collaboration has presented new activity and prompt results [14,15].

Our experiment was designed to measure both the prompt γ rays and the ^{7}Be activity produced in the same irradiation. The prompt γ yield was measured with a Ge detector at 90° with respect to the beam axis. To contain the ^{7}Be activity with a high efficiency and accurately define the active volume, we used a ^{3}He gas cell target 29.7 mm long with a thin, 1-μm nickel entrance foil. Gas pressures of 100 and 200 torr were used. The copper beam stopper at the end of the gas cell was removed after ^{4}He irradiation and counted together with the thin Ta gas cell liner to determine the ^{7}Be activity. We measured the cross section in the range $E_{\text{c.m.}} = 0.33$ to 1.23 MeV with statistical uncertainties of 3% or less for each data point and an overall systematic uncertainty of 3% for the activity data and 3.5% for the prompt data.

II. EXPERIMENTAL PROCEDURE

A. Experimental apparatus and procedure

We measured the ^{3}He + ^{4}He fusion cross sections using the Model FN Tandem Van de Graaff accelerator at CENPA, the Center for Experimental Nuclear Physics and Astrophysics, at the University of Washington. ^{4}He$^+$ beams of 1.5–3.5 MeV were produced in an rf-discharge ion source mounted in the terminal of the accelerator. The beam current on the target cell was typically 450–500 nA, which, together with beam rastering (see below), was designed to achieve good entrance foil lifetime. Between the switching magnet and the ^{3}He gas target, the beam passed through two magnetic quadrupole doublets, a set of X–Y magnetic rastering coils, and two LN_2 traps. A 7-mm water-cooled aperture was located just downstream of the second LN_2 trap. A second water-cooled 7-mm aperture was located 17 cm further downstream on a movable aperture plate, shown on the left side of Fig. 2. The beam then passed through two 8-mm-diameter cleanup collimators, through a cylindrical electron suppressor, through the 1-μm nickel entrance foil mounted on a nickel foil holder (with a 10-mm-diameter aperture), and into the cell as shown in Fig. 2. The apertures and collimators were made from Oxygen-Free High Conductivity (OFHC) copper and the beamline and the region immediately upstream of the gas cell were pumped by cryopumps.

The beam was tuned by focusing through a 1-mm-diameter aperture located on the movable aperture plate and backed by a tuning beam stop (see Fig. 2). Then the beam was rastered to a square distribution somewhat larger than 7 × 7 mm using 19-Hz and 43-Hz X and Y raster frequencies and sent through the 7-mm-diameter movable aperture into the gas cell.

The cell consisted of an aluminum cylinder with a 32-mm inside diameter, a 29.7-mm active length, and a 30-mm-diameter, 0.25-mm-thick OFHC copper beam stop soldered onto a copper back plate. The choice of OFHC copper for the beam stop was motivated by its low prompt background, low Li and B contamination, and small backscattering probability for low energy ^{7}Be ions. The back plate was air-cooled, and the cell wall was lined with 0.025-mm-thick Ta foil to catch ^{7}Be recoils that did not end up in the stopper.

Prompt γ rays were detected in an N-type Ge detector with 100% relative efficiency located at 90° with its cryostat front face ≈5 cm from the center of the cell. A 3.2-mm-thick Plexiglass absorber was placed between the cell and the detector to ensure that β particles in coincidence with γ rays from calibration sources did not penetrate into the Ge. The Ge detector was uncollimated and shielded on the sides by

*Present address: HH-NIPNE, Bucharest, Romania.
†snover@u.washington.edu

 ©2007 The American Physical Society

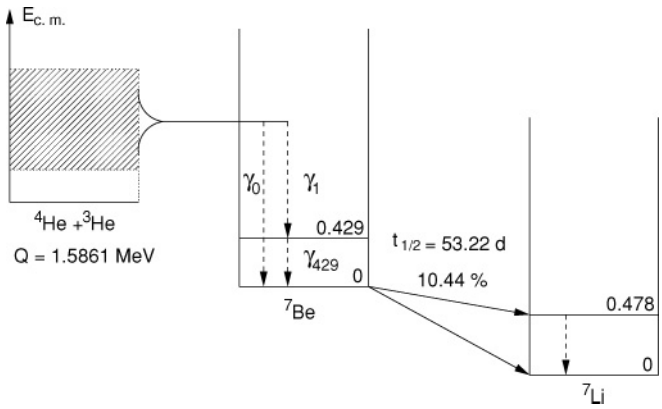

FIG. 1. Energy level diagram.

20 cm of Pb and on the rear by a partial 10-cm Pb shield. We determined the total prompt ^{3}He(^{4}He,γ)^{7}Be cross section from the γ_0 yield and the relatively sharp, isotropic 429-keV secondary following γ_1 emission. We used the γ_0 photopeak centroid to determine the mean reaction energy. ^{4}He $+^4$He background measurements were made at each bombarding energy to determine the prompt γ-ray background and provide a check on possible contaminant ^{7}Be production.

After irradiation, the stopper was removed from the back plate using a knife, and the delayed 478-keV γ rays from ^{7}Be decay in the stopper and the Ta liner were counted together in a close geometry using a second (offline) 100% Ge detector in an enclosed 20-cm-thick Pb shield.

B. Ge calibration

The Ge detectors were calibrated using ^{54}Mn, ^{60}Co, ^{133}Ba, ^{137}Cs, ^{88}Y, ^{113}Sn, and ^{203}Hg sources with activities in the range 1–7 kBq specified to an accuracy of $\pm$(0.7–1.2)% (1σ) [16]. We also used ^{7}Be and ^{24}Na sources made by the ^{10}B(p,α)^{7}Be and ^{23}Na(d,p)^{24}Na reactions. PENELOPE [17] Monte Carlo simulations were used to calculate finite source size correction factors for the online detector. The source line intensities were determined from asymmetric Gaussian function fits to the photopeaks. The energy calibration of the online detector

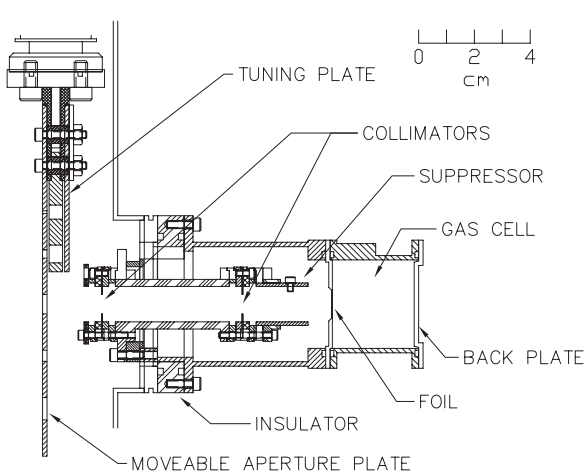

FIG. 2. Gas cell and beam collimation geometry.

was determined using *in situ* naturally occurring γ-ray lines, particularly the 1460.85- and 2614.55-keV lines from ^{40}K and ^{208}Tl decay.

1. *Offline (activity)* Ge *detector*

The offline Ge detector efficiency was measured in two ways. First, the ^{7}Be source strength was determined using the online Ge detector together with the calibrated sources listed above, at a source-to-detector distance of 25 cm, large enough that γ-γ summing was unimportant. Then the ^{7}Be source was used to calibrate the offline Ge in the close geometry, approximately 2.7 mm from the front face of the carbon fiber cryostat window. Second, the ^{54}Mn, ^{113}Sn, and ^{203}Hg calibration sources were used to calibrate the close geometry. The results of these two methods agreed well, with an absolute efficiency determination at 478 keV of typically 0.1246 ± 0.0015. A measured $\pm$0.25-mm longitudinal variation in source and stopper placement resulted in an additional $\pm$1% systematic error for the different measurements based on a measured efficiency sensitivity of 4% per mm displacement. A TRIM [18] calculation indicated that the spatial profile of the ^{7}Be implanted in the stopper was approximately a 9-mm-diameter disk. We included a 0.997 correction factor for this effect based on off-axis ^{7}Be source efficiency measurements.

TRIM calculations for our beam energies and foil and gas thicknesses indicated that >99% of the ^{7}Be atoms produced by ^{3}He + ^{4}He $\rightarrow$ ^{7}Be should be implanted in the beam stop. Because Be adheres readily to surfaces, any remaining ^{7}Be should have deposited on the interior surfaces of the cell, of which 80% was represented by the beam stop plus the Ta liner.

We counted the ^{7}Be activity with the stopper mounted as described above and the Ta liner cut up and mounted directly behind the stopper. In this geometry the γ rays from the liner were counted with an efficiency reduced by 5% due to the greater source-to-detector distance as well as absorption in the stopper and Ta. Separate measurements for several bombarding energies in which only the Ta liner was counted indicated <2% for the fraction of ^{7}Be activity on the liner; thus the reduced efficiency for counting the liner resulted in a negligible additional uncertainty. Our overall systematic uncertainty in the efficiency for counting the ^{7}Be activity was $\pm$1.6%. We assumed a ^{7}Be half-life of (53.22 ± 0.06) d and a (10.44 ± 0.04)% branching ratio for decay to the 478-keV daughter state [19].

2. *Online (prompt)* Ge *detector*

Online Ge detector efficiency measurements in the range $E_\gamma = 280$ to 2754 keV were made using the ^{24}Na, ^{54}Mn, ^{60}Co, ^{137}Cs, ^{88}Y, ^{113}Sn, and ^{203}Hg sources mounted in the center of the gas cell. For the two-line sources, summing corrections of up to (5 ± 1)% were made based on measured peak/total ratios and computed γ-γ angular correlation coefficients. The results, shown in Fig. 3, determine the online detection efficiency to $\pm$1.6%. The position of the online detector was not exactly the same for the measurements at different bombarding energies. We assigned an additional $\pm$1% variable

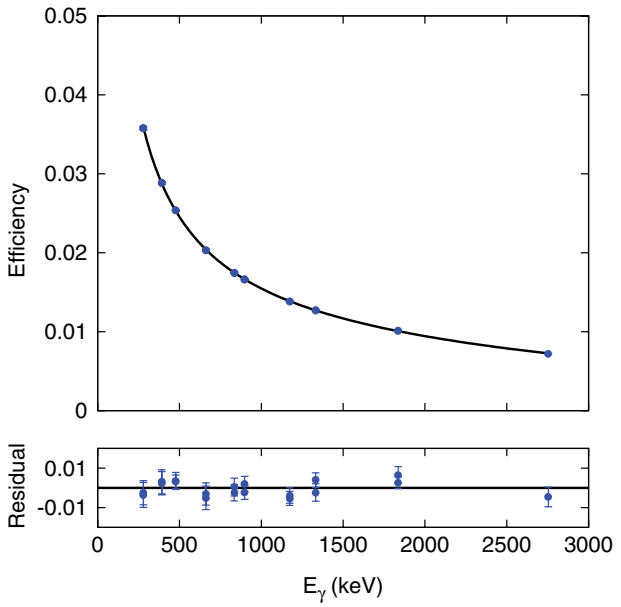

FIG. 3. (Color online) Absolute online Ge photopeak detection efficiency vs E_γ. Solid points are measurements. Error bars are statistical. The curve is the fit to the data of the function $\epsilon(E_\gamma) = aE_\gamma^b(1 + cE_\gamma^2)$, with a, b, and c parameters. (Bottom panel) Fractional fit residuals.

systematic error to its efficiency based on numerous repeat efficiency measurements.

We made additional efficiency measurements with the sources mounted inside the cell and displaced along its axis, as shown in Fig. 4. Increased absorption causes the efficiency to drop near the foil holder and near the back plate. The measured dependence of efficiency on displacement is reproduced well by the PENELOPE [17] Monte Carlo efficiency simulations described below.

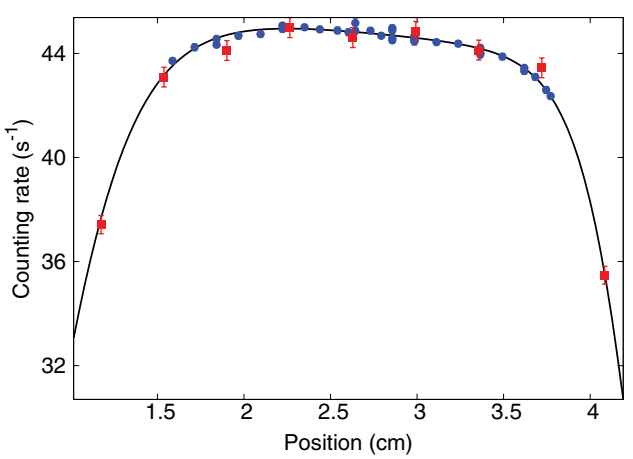

FIG. 4. (Color online) Solid (blue) circles are measured online Ge detector efficiency vs position for a ^{137}Cs source on the axis of the gas cell. Solid (red) squares are PENELOPE simulations. The curve is to guide the eye. The center of the cell is at 2.63 cm, the simulated end points are located at positions near the ends of the cell, and the position scale has an arbitrary offset.

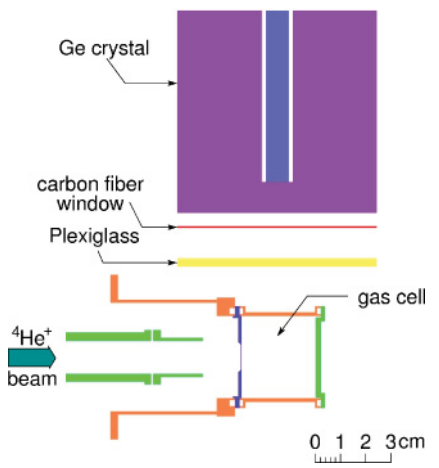

FIG. 5. (Color online) Gas cell and detector geometry used in PENELOPE simulations. The beam enters from the left, passing through the collimator mounting tube and electron suppressor. The Ge detector is shown with its carbon fiber window and Plexiglass absorber.

The γ_0 yield was obtained by summing the counts in a background-subtracted window around the full-energy peak, and the 429-keV yield was determined by fitting the peak shape with the same function used for fitting the source lines and the 478-keV line.

3. PENELOPE *Monte Carlo efficiency calculations*

Prompt γ rays were emitted from an extended cylindrical volume inside the gas cell. The prompt γ_0 energy distribution was broadened by beam energy loss in the gas and by the Doppler shift, and as a result the broad γ_0 peak contained a 2–3% Compton scattering component. To account accurately for these effects we carried out detailed efficiency simulations using the PENELOPE computer code [17].

Figure 5 shows the detector and gas cell geometry used in the PENELOPE calculations. Because we needed simulated γ-ray spectra only for energies near the photopeak, we included only materials that resulted in line-of-sight absorption and/or small angle forward scattering between the cell and the detector. Detector properties were taken from manufacturer's specifications [20]. Efficiency simulations for the calibration source energies were typically 5–7% higher than our measurements for $E_\gamma = 0.4$–3.0 MeV.

We modeled the γ_0 detection efficiency using TRIM to calculate the energy and position dependence of γ rays emitted from the gas cell for each bombarding energy. The measured Ni foil thickness, ^{3}He gas pressure, and accelerator beam energy were inputs for these calculations. The variation of cross section with energy was included by assuming a constant S factor over the range of energy loss in the cell. The result of these calculations served as input for the PENELOPE simulation. In general the simulated line shapes agreed very well with the data, as can be seen for the $E_{\text{c.m.}} = 0.43$ MeV case shown in Fig. 6.

To minimize our sensitivity to calculations, we used PENELOPE efficiency simulations only for ratios that are close to unity. We determined the γ_0 and γ_{429} detection efficiencies

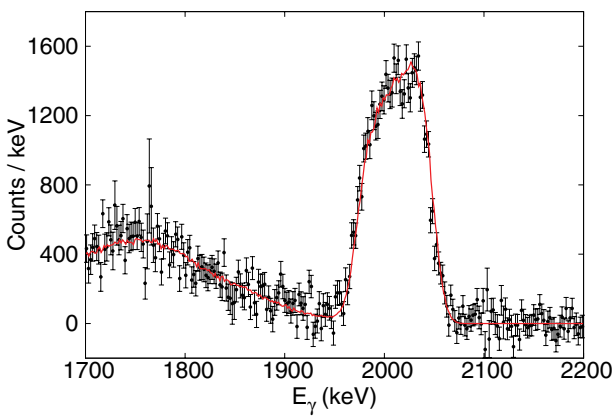

FIG. 6. (Color online) $E_{\text{c.m.}} = 0.43$ MeV ($E_\alpha = 1.7$ MeV) prompt background-subtracted γ spectrum (points) and PENELOPE simulation (curve) in the region of the γ_0 peak.

$\epsilon(E_\gamma)$ from the relation

$$\epsilon(E_\gamma) = \epsilon_p(E_\gamma)\frac{\epsilon'_d(E_\gamma)}{\epsilon'_p(E_\gamma)}, \tag{1}$$

where $\epsilon_p(E_\gamma)$ is the point-source efficiency measured at the center of the cell, $\epsilon'_d(E_\gamma)$ is the PENELOPE distributed-source efficiency, $\epsilon'_p(E_\gamma)$ is the PENELOPE point-source efficiency, and E_γ is the mean γ-ray energy. Small (several keV) inaccuracies in the simulated γ_0 energy distribution were taken into account by adjusting the window used to sum the simulated yield by the difference in the measured and simulated γ_0 centroids. The calculated PENELOPE efficiency ratios were all within 4% of unity. This, together with the fact that the measured and simulated point-source efficiencies agree well as described above, suggests a systematic uncertainty on the simulated efficiency ratio that is less than the typical simulation statistical uncertainty of ≈0.4%.

C. Beam current integration

We determined the number of α particles entering the gas cell by integrating the electrical current measured on the gas cell, including foil holder and cell support tube, which acted as a Faraday cup as shown in Fig. 2. Beam collimation and alignment ensured that the beam passed cleanly through the foil holder aperture. Secondary electron loss from the foil was suppressed with −600 V applied to the electron suppressor. The (negative) current on the last (8 mm) collimator just upstream of the suppressor was always less than 1% in magnitude compared to the (positive) cell current. The current integrator was checked to a precision of better than 1% with two different precision dc current sources and with a square wave generator.

We also made measurements without foil or gas, in which we compared the integrated beam current with the integrated beam power determined with a calorimeter suitable for relative measurements. We used both proton and $^4He^+$ beams at 1.00 MeV, and we compared a geometry close to that used for the cross section measurements with a different Faraday cup geometry. In all these comparisons, the ratio of the number of beam particles determined from the integrated beam current and from the integrated beam power was the same within the measurement accuracy of ±1%.

A potential concern is the possiblity of He^+ charge-changing collisions in the residual gas of the beamline upstream of the target. Pickup is negligible compared to stripping [21], and the strong defocusing effect of the beam transport, which would transmit less than 1% of a He^{++} beam when tuned for He^+ ions, indicates that only those He^{++} ions produced in the 2-m beamline section downstream of the last quadrupole lens may reach the target cell. In this region the beamline pressure was $< 2 \times 10^{-6}$ torr. The stripping cross section on O_2 and N_2 shows a broad maximum at $E_\alpha \approx 1.0$ MeV and a peak cross section of $\approx 1.6 \times 10^{-16}$ cm^2 [21]. These parameters imply the fraction of He^{++} ions reaching the target was <0.2%. The rastering would reduce the He^{++} fraction by an additional factor of ≈ 4; hence He^+ charge-changing collisions were not an important concern for our measurements.

D. Target cell gas and foil properties

The nickel entrance foils were 1-μm in nominal thickness, glued onto the nickel foil holders. Fresh foils were used for most bombarding energies. Foil thicknesses were measured to ±1% using the 3.2-MeV α particles from ^{148}Gd. Most foils leaked He at a slow rate, and the cell pressure was "topped off" to maintain a constant average pressure over time. Pressure variations over the course of a 1-h irradiation were < 6%. The increase in cell depth due to foil bulge was measured to be 0.3–0.4 mm averaged over the 7- to 8-mm beam diameter.

We used ^{3}He gas with 99.999% (99.99%) chemical (isotopic) purity and naturally occurring He gas with 99.9999% chemical purity. The cell was flushed with ^{3}He (or ^{4}He) before and during the cross section measurements, which were carried out at nominal pressures of 200 torr (two highest energies) and 100 torr. Gas purity was measured *in situ* after some time in the cell, using a residual gas analyzer and found to > 99% pure. Gas pressure was measured with a Baratron [22], whose precision was checked with a mercury manometer to better than 1% at 100–200 torr, and was recorded in 1-s time intervals with an ADC (Analog-to-Digital Converter). Cell temperature was measured with an insulated probe attached to the cell wall and recorded at the beginning and end of each 1-h run.

E. Contaminant ^{7}Be production

As Hilgemeier *et al.* [9] pointed out, ^{7}Be may be produced by a background process, e.g., ^{6}Li(d,n)^{7}Be or ^{10}B(p,α)^{7}Be if there is both a (proton or deuteron) contamination in the ^{4}He beam and a (^{6}Li or ^{10}B) contaminant in the gas cell, e.g., the foil or beam stop. This concern was apparently overlooked in earlier ^{3}He + ^{4}He →^{7}Be activity measurements. We guarded against this possibility by counting the stoppers from the ^{4}He +^{4}He irradiations for five of the eight bombarding energies. We obtained 1–2% upper limits (1σ) on contaminant ^{7}Be production from each of these measurements.

To understand the possible magnitude of this problem in older ^{3}He + ^{4}He →^{7}Be activity measurements, we made a study of beam and target stopper impurities. Using our 90° analyzing magnet and a 3-MeV $^4He^+$ beam, we found

TABLE I. Beam heating density correction factors, percent per 600 nA.

Case	E_{res} (MeV)	100 torr	200 torr
^{24}Mg(α, γ)^{28}Si	3.20	–	3.9 ± 0.6
^{10}B(α, $p-\gamma$)^{13}C	1.51	5.3 ± 0.8	7.8 ± 1.0

a D_2^+ and/or DH_2^+ satellite beam with intensity 0.1–1% (depending on source preparation) at slightly higher rigidity than the $^4He^+$ beam. Accelerator voltage instabilities, e.g., sparks, could allow this beam to pass through the analyzing magnet slits with a nonzero duty factor. We then bombarded various Co, Ni, Cu, Nb, Ta, Pt, and Au materials selected for good chemical purity (> 99.9%) with 0.75-MeV protons and 1.5-MeV deuterons (the energies that would result in the above example) and measured the ^{7}Be activity produced [23]. Our results suggest that contaminant ^{7}Be production in the older activity experiments was probably not significant. We note that the Osborne *et al.* [7] activity measurements were made with a Tandem accelerator in which the beam was stripped in the terminal and hence was unlikely to contain molecular impurities. We also note that a ^{3}He beam experiment is more dangerous because ^{7}Li(^{3}He,t) and ^{6}Li(^{3}He,d) reactions can lead to contaminant ^{7}Be production without the need for a beam contaminant.

F. Beam heating corrections

The region of the gas cell illuminated by the beam has a higher temperature and hence a lower density than the rest of the cell. We measured this effect using narrow resonances in the ^{24}Mg(α, γ)^{28}Si and ^{10}B(α, $p-\gamma$)^{13}C reactions at $E_{res} = 3.20$ and 1.51 MeV, respectively. We coated the gas-cell stopper with a thin layer of natural Mg or B and measured the thick-target resonance yield with and without the foil and gas. Then, with the foil and gas present, and the beam energy adjusted halfway up the leading edge of the resonance, we measured the resonance yield as a function of the beam current. The gas density correction factors determined from these data are shown in Table I. The beam heating corrections for our 200-torr ^{3}He + ^{4}He →^{7}Be measurements were determined by interpolating between the entries shown in Table I, while the 100-torr ^{3}He + ^{4}He →^{7}Be corrections were determined by extrapolating the 100-torr measurement, scaling by the calculated gas dE/dx (see Table II).

G. γ_0 anisotropy

The 429-keV γ ray following γ_1 emission is isotropic, because it proceeds from a $J = 1/2$ state; however, γ_0 need not be. Tombrello and Parker [24] calculated the angular anisotropy, which they found to be small but nonzero in our energy range. Column 6 of Table III shows the 90° γ_0 anisotropy correction factors $1/(1 - a_2 Q_2/2)$ calculated from Ref. [24], where a_2 is the coefficient of the Legendre polynomial P_2 and $Q_2 = 0.9$ is the angular attenuation coefficient for our geometry. These corrections range from 0.99 to 1.04 for our energies. Kim, Izumoto, and Nagatani [25] calculated the γ_0 angular distribution at several energies; at $E_{c.m.} = 0.1$ MeV their result agrees well with that of Ref. [24] while at $E_{c.m.} =$ 1 MeV their result corresponds to an anisotropy correction factor 2% larger than that of Ref. [24].

The angular distribution is sensitive to the phase difference between s- and d-wave capture amplitudes, which has not been measured in our energy range. Both calculations assumed a hard-sphere extrapolation of the nuclear part from data at higher energies, where measurements are consistent at the level of 5° [26]. We estimate that a 5° change in this phase difference would give rise to a 2% change in the anisotropy correction at our energies, on average. Thus it seems reasonable to assume a ±2% uncertainty in this correction. We note that Kräwinkel *et al.* [6] are the only ones to have measured the anisotropy, and their results do not constrain it at this level of precision.

III. RESULTS

We measured the ^{3}He + ^{4}He →^{7}Be fusion cross section at eight bombarding energies from $E_{c.m.} = 0.33$ to 1.23 MeV. Some properties of these measurements are shown in Table II. At each bombarding energy we measured the ^{4}He +^{3}He yield

TABLE II. Conditions of the cross section measurements.

$E_{c.m.}$ (MeV)	E_α (MeV)	Foil (μm)	ΔE_{foil} (MeV)	P_{gas} (torr)[a]	ΔE_{gas} (MeV)	I_{av} (nA)	BH (%)[b]	T_{irrad} (h)[c]	T_{act}(d)[d]
0.3274	1.5	0.968	0.677	100	0.166	480	5.3	102.3	26.6
0.4260	1.7	0.937	0.641	100	0.158	460	4.9	116.5	12.0
0.5180	1.9	0.955	0.638	100	0.148	450	4.5	30.9	33.6
0.5815	2.1	1.069	0.691	100	0.141	420	3.9	24.4	20.5
0.7024	2.35	1.069	0.665	100	0.129	450	3.9	23.3	10.4
0.7968	2.6	1.072	0.642	200	0.240	500	5.9	20.3	7.2
1.2337	3.5	1.065	0.545	200	0.182	440	3.5	14.7	6.8
1.2347	3.5	1.051	0.538	200	0.182	120/500	1.2/4.9	41.8	31.8

[a]Nominal gas pressure.
[b]Average beam heating correction.
[c]^{4}He +^{3}He irradiation time.
[d]Activity counting time.

TABLE III. Our S factors, prompt γ-ray branching ratios, and calculated γ_0 anisotropy.

$E_{c.m.}$ (MeV)	S_{act} (keV b)[a]	S_{prompt} (keV b)[a,b]	S_{prompt}/S_{act}[b]	γ_{429}/γ_0[b]	Anisotropy[c]
0.3274 ± 0.0013	0.495 ± 0.015	0.492 ± 0.014	0.994 ± 0.042	0.410 ± 0.023	0.988
0.4260 ± 0.0004	0.458 ± 0.010	0.438 ± 0.006	0.956 ± 0.024	0.405 ± 0.009	1.002
0.5180 ± 0.0005	0.440 ± 0.010	0.421 ± 0.007	0.957 ± 0.026	0.394 ± 0.009	1.013
0.5815 ± 0.0008	0.400 ± 0.011	0.398 ± 0.008	0.995 ± 0.035	0.422 ± 0.013	1.019
0.7024 ± 0.0006	0.375 ± 0.010	0.382 ± 0.006	1.020 ± 0.031	0.424 ± 0.010	1.030
0.7968 ± 0.0003	0.363 ± 0.007	0.371 ± 0.004	1.022 ± 0.023	0.427 ± 0.005	1.036
1.2337 ± 0.0003	0.330 ± 0.006	0.327 ± 0.004	0.990 ± 0.021	0.439 ± 0.006	1.040
1.2347 ± 0.0003	0.324 ± 0.006	0.340 ± 0.004	1.050 ± 0.023	0.443 ± 0.007	1.040

[a]Uncertainties include statistics, $\pm 1\%$ variable systematic, and the contribution from the $E_{c.m.}$ uncertainty.
[b]Assuming γ_0 isotropic.
[c]γ_0 anisotropy correction $1/(1 - a_2 Q_2/2)$ calculated from Ref. [24].

in a series of 1-h runs for the total time indicated. The rastered beam current on the cell was 420-500 nA.

^{4}He $+^4$He background measurements were also made at each bombarding energy, for an irradiation time 60–130% of the ^{4}He $+^3$He irradiation time. Some background increase with time was observed for most of the runs, which we attributed mainly to the ^{13}C(α,n)^{16}O reaction on carbon buildup. ^{4}He $+^4$He measurements were made before and after the ^{4}He $+^3$He measurements and were summed to correct, to first order, for the prompt γ-ray background increase with irradiation time. Separate stoppers were used for the ^{4}He $+^3$He and ^{4}He $+^4$He irradiations so we could count the ^{4}He $+^4$He stoppers to check for contaminant ^{7}Be production (see Sec. II E).

The γ-ray spectra measured at $E_{c.m.} = 1.23$ and 0.43 MeV are shown in Figs. 7 and 8. For most of the measurements the beam-related background (per μC) determined from ^{4}He $+^4$He was statistically consistent with the background observed above the γ_0 peak in the ^{4}He $+^3$He spectra. Even so, we adopted a more conservative procedure of determining the ^{4}He $+^3$He background by normalizing the (beam-related part of the) ^{4}He $+^4$He spectrum to a region above the γ_0 peak in the ^{4}He $+^3$He spectrum. The ^{4}He $+^4$He spectra shown in the top panels of these figures are shown with this normalization. The lower panels in Figs. 7 and 8 show the background-subtracted prompt spectra in the region of the γ_0 and 429-keV peaks, and they show the window used to sum the γ_0 counts. Sharp features in the subtracted spectra near 2614 and 1765 keV originate from large background peaks that have

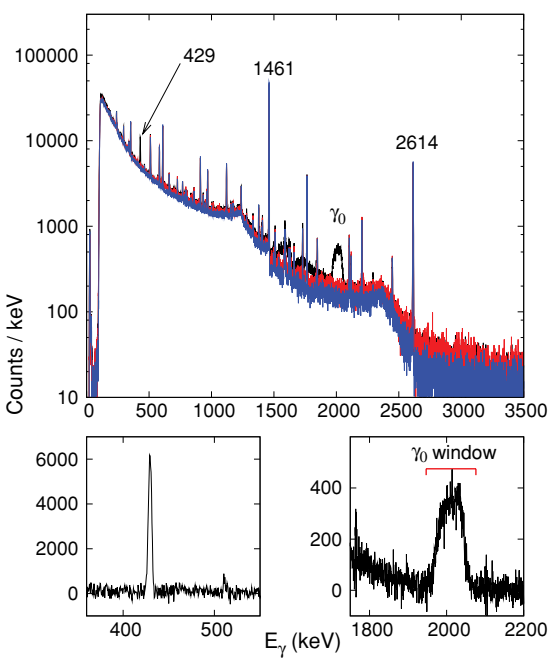

FIG. 7. (Color online) Prompt γ spectra measured at $E_\alpha = 1.7$ MeV ($E_{c.m.} = 0.43$ MeV). (Top panel, from top to bottom) ^{4}He $+^3$He (black), ^{4}He $+^4$He (red), and beam-off background (blue) spectra. (Bottom panels) Background subtracted spectra in the region of the 429 keV line and γ_0. The window used to determine the γ_0 yield is indicated.

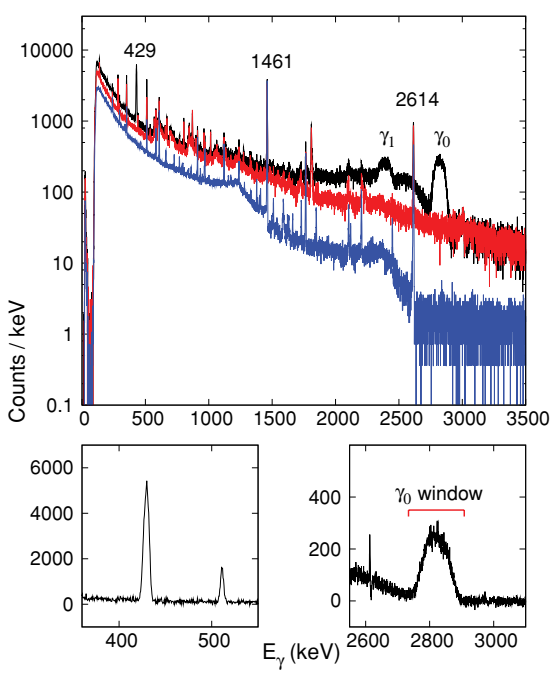

FIG. 8. (Color online) Prompt γ spectra measured at $E_\alpha = 3.5$ MeV ($E_{c.m.} = 1.23$ MeV). The colors correspond to those used in Fig. 7. See legend to Fig. 7 for additional information.

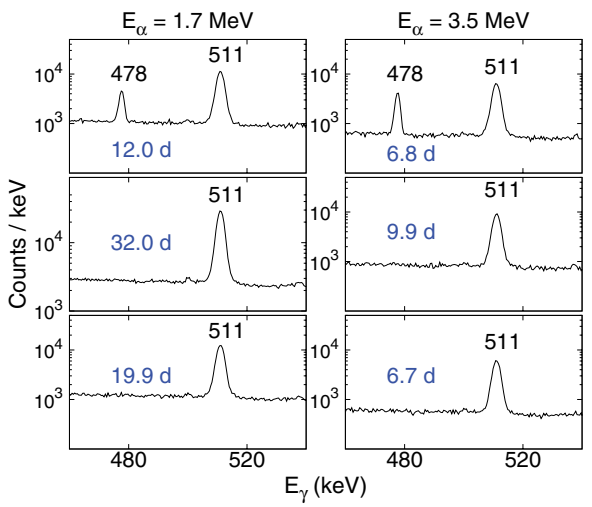

FIG. 9. (Color online) $E_{\text{c.m.}} = 1.23$ and 0.43 MeV ($E_\alpha = 1.7$ and 3.5 MeV) offline activity spectra. (Top panels) ^{4}He +^{3}He irradiation. (Middle panels) ^{4}He +^{4}He irradiation. (Bottom panels) Source-out background. Counting periods (in d) are shown.

been subtracted imperfectly (due to small gain shifts) and have small net areas.

In our $E_{\text{c.m.}} = 0.80$ MeV data we observed a large carbon buildup. This allowed us to check that the beam-related backgrounds due to carbon buildup and the background present before buildup had the same shape in the region of interest. Thus our method of background determination under the prompt γ_0 peak appears to be robust.

The $E_{\text{c.m.}} = 1.23$ and 0.43 MeV activity spectra are shown in Fig. 9. Neither the source-out background (measured with a Cu stopper that had not been irradiated) nor the ^{4}He +^{4}He stopper measurements showed any sign of a 478-keV peak.

We determined the mean reaction energy from the γ_0 centroid. The advantage of this method is that it does not depend on knowledge of the beam energy or the energy loss in the foil or gas, and it is determined directly from the events used to determine the cross section. However, the broad γ_0 peak contains a small forward-angle Compton scattering component in addition to the majority of events in which the full γ-ray energy is deposited in the Ge. The γ_0 centroid must be corrected for this component to obtain the mean reaction energy. [Note that the Compton contribution to the γ_0 detection efficiency is included in the PENELOPE ratio factor that appears in Eq. (1)]. We computed centroid corrections of 1.2 ± 0.1 and 1.9 ± 0.1 keV for the $E_{\text{c.m.}} = 0.33$ and 1.23 MeV cases using the measured detector response for $E_\gamma = 1836$ and 2754 keV, and we interpolated linearly to obtain the corrections for the other reaction energies. These corrections shift our inferred S factors down by 1.2% (0.9%) for the $E_{\text{c.m.}} = 0.33(0.43)$ MeV cases and less at the higher energies.

We also corrected for a small net positive Doppler shift in the γ_0 centroid. This resulted primarily because, on average, the γ rays were emitted somewhat ($\leqslant$2 mm) upstream of the center of the cell. The calculated correction is 0.35 (0.2) keV for the $E_{\text{c.m.}} = 0.33(0.43)$ MeV cases and has the sign opposite that of the Compton correction discussed above. All of our quoted $E_{\text{c.m.}}$ values and S factors include these corrections.

As an additional check on beam current integration, we remeasured the cross section at $E_{\text{c.m.}} = 1.23$ MeV using 4-mm-diameter instead of 7-mm-diameter beam-defining apertures. This further minimized the secondary electron currents on the cleanup collimators. We determined the beam heating correction for this collimation geometry directly from ^{3}He + ^{4}He → ^{7}Be data measured at 120 and 500 nA. The good agreement between the activity S factors deduced from these two $E_{\text{c.m.}} = 1.23$ MeV cross section measurements provides additional evidence that our beam current integration and beam heating estimates are reliable. The prompt S factors for the two 1.23 MeV measurements agree less well; however, here we measured the ^{4}He +^{4}He beam-related background only at 500 nA.

A. *S* factors

Our measured S factors are shown in Table III. The mean center-of-mass reaction energy was determined by subtracting the 1586.1 ± 0.1 keV Q value [27] from the γ_0 centroid. Cross sections were converted to S factors using the relation

$$S(E_{\text{c.m.}}) = \sigma(E_{\text{c.m.}}) E_{\text{c.m.}} e^{(E_G/E_{\text{c.m.}})^{1/2}}, \tag{2}$$

with $E_G^{1/2} = 164.13$ keV$^{1/2}$. The tabulated uncertainties in the S factors and their ratios include statistics, the $\pm 1\%$ variable systematic uncertainties shown in Table IV, and the contribution of the uncertainty in the mean reaction energy $E_{\text{c.m.}}$—the latter is important only at the lowest bombarding energy. We also show the experimental branching ratio $\gamma_{429}/\gamma_0 (= \gamma_1/\gamma_0)$ and the anisotropy calculated from Ref. [24] (see Sec. II G).

Table IV shows the sources of systematic uncertainty and their contributions to the S-factor uncertainty. The $\pm 1\%$ variable systematic uncertainties given in Table IV are included

TABLE IV. Systematic uncertainties $\Delta S(E_{\text{c.m.}})/S(E_{\text{c.m.}})$. The variable uncertainties are assumed random between the various $S(E_{\text{c.m.}})$ values, while the scale factor uncertainties are the same for all the values.

	Type[a]	ΔS/S%	Origin
Variable	a, p	1.0	Source positioning
Scale factor	a, p	1.6	Ge efficiency[b]
	p	1.0	Beam centering
	p	1.5	γ_0 anisotropy
	a, p	1.6	Current integration
	a, p	1.3	Gas pressure
	a, p	0.6	Temperature
	a, p	0.7	Gas purity
	a, p	0.4	Gas cell length[c]
	a, p	1.0	Beam heating
Total scale factor	a	3.0	
	p	3.5	
	Common	2.7	

[a]Activity and/or prompt.
[b]Prompt value includes summing and simulation uncertainties.
[c]Includes foil bulge.

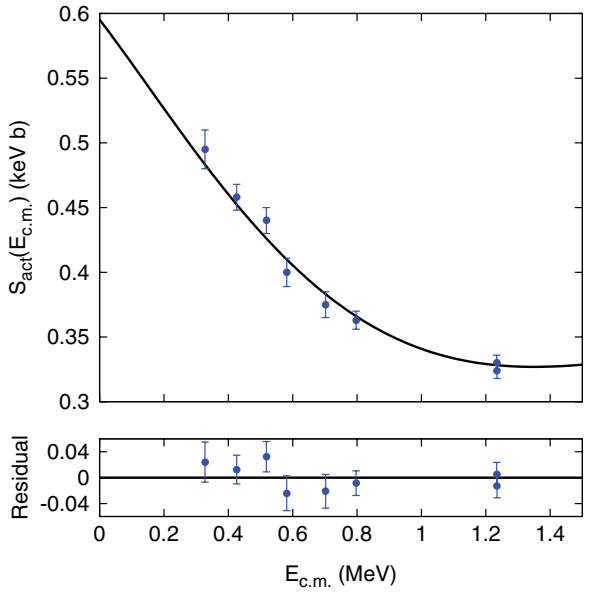

FIG. 10. (Color online) Solid (blue) points are $S_{act}(E_{c.m.})$ vs $E_{c.m.}$. The curve is the fit of Kajino's function. (Bottom panel) Fractional fit residuals.

in the S-factor values and ratios shown in Table III and in the fitting of $S(E_{c.m.})$ vs $E_{c.m.}$, while the systematic scale-factor uncertainty is folded with the fit uncertainty to give the total uncertainty. The fit uncertainties include the factor $\sqrt{\chi^2/\nu}$ whenever $\chi^2/\nu > 1$.

Figure 10 shows $S_{act}(E_{c.m.})$ vs $E_{c.m.}$ together with a fit in which the theoretical shape given by Eq. (6) of Kajino, Toki, and Austin [28] has been scaled to fit the data. Figure 11 shows $S_{prompt}(E_{c.m.})$ based on an assumed isotropic angular distribution for γ_0 together with the Kajino fit. In these fits the

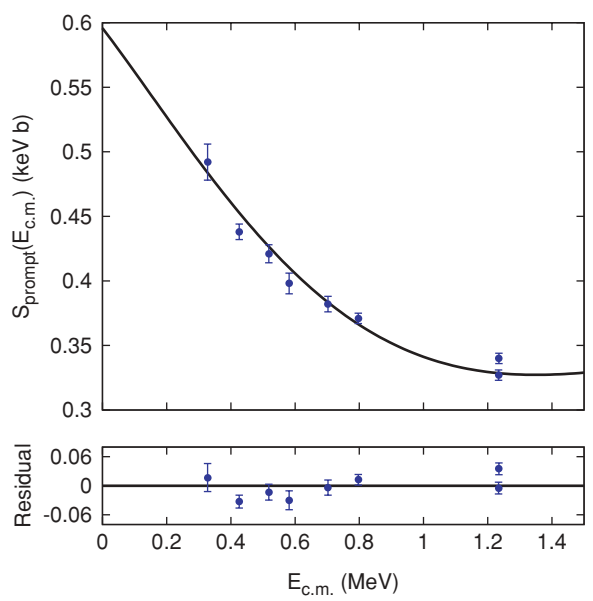

FIG. 11. (Color online) Solid (blue) points are $S_{prompt}(E_{c.m.})$ vs $E_{c.m.}$, for the isotropic γ_0 assumption. The curve is the fit of Kajino's function. (Bottom panel) Fractional fit residuals.

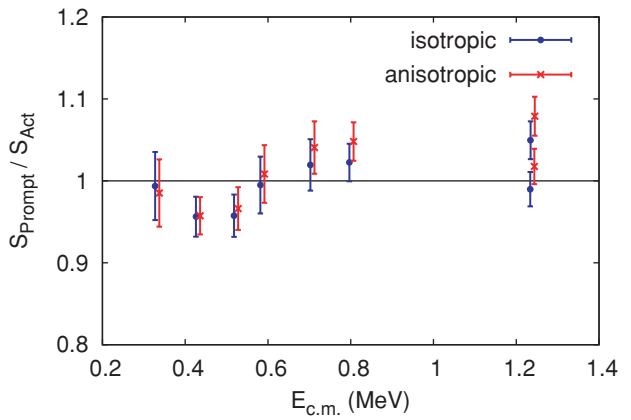

FIG. 12. (Color online) S_{prompt}/S_{act} vs $E_{c.m.}$. (Solid blue circles) Assuming γ_0 isotropic. (Red x's) γ_0 corrected for theoretical anisotropy as given in Table III. The crosses have been displaced from the circles for clarity.

shape parameters of the fit function are held constant and only one parameter, $S(0)$, is varied.

Figure 12 shows the ratios S_{prompt}/S_{act} for both the isotropic and anisotropic assumptions for γ_0. We fit the ratios S_{prompt}/S_{act} vs $E_{c.m.}$ with a horizontal line, and we also fit our $S_{prompt}(E_{c.m.})$ values based on the anisotropic assumption. The results of all these fits are shown in Table V, including the confidence level $P(\chi^2, \nu)$ for each fit. The fit to $S_{act}(E_{c.m.})$ has a good quality. The fit to $S_{prompt}(E_{c.m.})$ is very poor quality for the anisotropic case, and although the confidence level is still low, it's much better for the isotropic assumption. The ratio fits are also poorer for the anisotropic assumption and acceptable for the isotropic assumption. Thus we conclude that the γ_0 anisotropies calculated from Ref. [24] are not consistent with our data, while the isotropic approximation is better. Thus our best $S(0)$ values based on the Kajino fit function are

$$S_{act}(0) = 0.595 \pm 0.018\,\text{keV b}, \tag{3}$$

and

$$S_{prompt}(0) = 0.596 \pm 0.021\,\text{keV b}. \tag{4}$$

Our best value for $S(0)$ is obtained by combining the activity and prompt results given above, taking into account the 2.7%

TABLE V. Our $S(0)$ values and prompt/activity ratios.

Quantity	Value[a]	χ^2/ν[b]	P(%)[c]
$S_{act}(0)$	0.595 ± 0.018 keV b	0.72	65
$S_{prompt}(0)$[d]	0.596 ± 0.021 keV b	2.7	1
S_{prompt}/S_{act}[d]	0.999 ± 0.030	1.8	9
$S_{prompt}(0)$[e]	0.607 ± 0.022 keV b	5.3	0.0004
S_{prompt}/S_{act}[e]	1.015 ± 0.032	2.9	0.5
Combined $S(0)$[f]	0.595 ± 0.018 keV b		

[a]Uncertainties include systematic contributions.
[b]$\nu = 7$.
[c]$P(\chi^2, \nu)$ is the confidence level of the fit.
[d]γ_0 assumed isotropic.
[e]γ_0 corrected by theoretical anisotropy—see Table III.
[f]Activity and isotropic prompt.

common scale factor uncertainty given in Table IV:

$$S(0) = 0.595 \pm 0.018\,\text{keV b}. \quad (5)$$

IV. COMPARISON WITH OTHER EXPERIMENTS

We found that fitting a given data set with different theories resulted in $S(0)$ values that varied typically by several percent (5% in the case of Ref. [10], which consists of one high-energy point). Hence in comparisons of different experimental results, it is important to use the same fitting function—the exceptions are the LUNA results [14,15], which were determined from data at very low energy. Because the resonating-group calculations of Kajino *et al.* [28] do a good job of reproducing other observables, and result in a reasonable theoretical value for $S(0)$, we chose this fit function. We obtained data from the original publications, from the NACRE compilation [29], and from other sources (see Refs. [4,7]).

The results are shown in Table VI. Most differences between the earlier results shown here and in Table II of Ref. [12] are due to the differing fitting functions; the notable exception is the Osborne *et al.* [7] activity result, which is significantly higher here. This problem has been noted before—see Kajino, Toki, and Austin [28] Table 1 and footnotes. We fit Osborne *et al.*'s $S_{\text{act}}(E_{\text{c.m.}})$ values quoted in their published Table 1 [7], which are the same as shown in their published Fig. 9 and in Osborne's Ph.D. thesis [7]. Volk *et al.* [11] give insufficient detail for us to interpret their integral measurement in a manner consistent with our other analyses; hence, we simply quote their published value.

TABLE VI. $S(0)$ values from our work and from published data.

	$S(0)$[a] (keV b)	Reference	
Activity	0.577 ± 0.035	Osborne *et al.*	[7]
	0.660 ± 0.040	Robertson *et al.*	[10]
	0.560 ± 0.030[a]	Volk *et al.*	[11]
	0.546[c] ± 0.020	Nara Singh *et al.*	[13]
	0.545 ± 0.017	Bemmerer *et al.*	[14]
	0.595 ± 0.018	Present work	
Prompt	0.481 ± 0.053	Parker and Kavanagh	[4]
	0.579 ± 0.07[d]	Nagatani *et al.*	[5]
	0.449 ± 0.06[e]	Kräwinkel *et al.*	[6]
	0.522 ± 0.03	Osborne *et al.*	[7]
	0.478 ± 0.04	Alexander *et al.*	[8]
	0.542 ± 0.03	Hilgemeier *et al.*	[9]
	0.560 ± 0.021	Confortola *et al.*	[15]
	0.596 ± 0.021	Present work	
Total[f]	0.560 ± 0.017[b]	Confortola *et al.*	[15]
	0.595 ± 0.018	Present work	

[a]From our fits of Kajino's function to published $S(E)$ values, with uncertainties as quoted by authors except where noted.
[b]Value and uncertainty as quoted by authors.
[c]Scaled by 1.008 to account for the different ^{7}Be decay BR assumed.
[d]Uncertainty as quoted in Ref. [12].
[e]Value corrected by ×1.4, and uncertainty as given in Ref. [9].
[f]Combined activity and prompt.

TABLE VII. $S(0)$ comparisons.

Data	S(0)[a]	χ^2/ν	ν	P(%)[b]
All activity	0.568 ± 0.014	2.1	5	6
All activity except [10]	0.563 ± 0.011	1.3	4	27
All prompt	0.549 ± 0.016	2.0	7	5
All[c]	0.559 ± 0.012	2.1	11	2
Present tot + [15] tot + [13]	0.568 ± 0.014	1.8	2	16
Present tot + [14] + [13]	0.562 ± 0.017	2.5	2	8

[a]All fit uncertainties contain the factor $\sqrt{\chi^2/\nu}$.
[b]$P(\chi^2, \nu)$.
[c]All except the last two prompt values and the last two activity values in Table VI.

The activity and prompt $S(0)$ values from Table VI are shown in Fig. 13 together with separate fits to the activity values and to the prompt values. These and other fit results are shown in Table VII. Our contaminant study reported in Sec. II E suggests earlier activity results probably did not suffer from contaminant ^{7}Be production. Earlier theoretical work showed that processes other than single-photon emission, such as $E0$ emission, should be negligible [30], while our measured prompt/activity ratios imply an experimental upper limit on $E0$ emission of ≈2%. Thus we see no reason why older activity measurements, as a group, should be flawed. However, as shown in Table VII, the fit to all activity values has a poor χ^2/ν and a poor confidence level, though an acceptable quality fit is obtained if the Robertson *et al.* datum [10] is removed.

Comparing recent measurements, our total (prompt + activity) $S(0)$ agrees with that of Confortola *et al.* [15] (see Table VI) and is higher than the activity results of Refs. [13,14], as shown in Fig. 14. Combining our total value with that of Ref. [15] and with the activity result of Ref. [13] yields a minimally acceptable fit; substituting the activity result of Ref. [14] for the Ref. [15] total value yields a similar result though the fit quality is not as good—see Table VII. Note that we do not include the results of both Refs. [14] and [15]

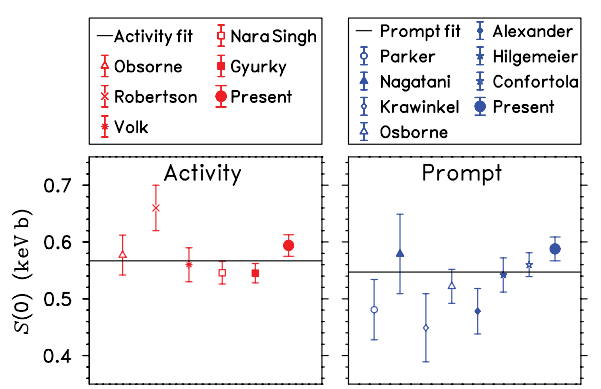

FIG. 13. (Color online) (Left panel) Red points, $S_{\text{act}}(0)$. (Right panel) Blue points, $S_{\text{prompt}}(0)$. The horizontal lines are the fits to the activity values (left panel) and prompt values (right panel) as given in Table VII.

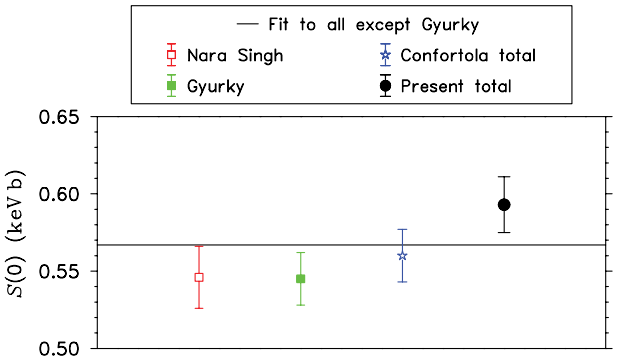

FIG. 14. (Color online) Recently measured $S(0)$ values. Points, from left to right: Ref. [13] and Ref. [14] activity values, Ref. [15], and present activity + prompt values. Horizontal line—fit to Ref. [13] values, Ref. [15] total, and present total as given in Table VII.

in the same fit because these values are presumably highly correlated, and the degree of correlation is not specified. We also did not derive an activity value for $S(0)$ from Ref. [15] for the same reason.

V. CONCLUSION

We have presented new results for the ^{3}He + ^{4}He $\rightarrow$ ^{7}Be S factor based on measurements of the prompt γ rays and the ^{7}Be activity produced in the same irradiation. We find good agreement between the two methods and a combined result,

$$S(0) = 0.595 \pm 0.018\,\text{keV b}, \tag{6}$$

based on fits of the theory of Kajino, Toki, and Austin [28] to our data.

The lack of good agreement between the various $S(0)$ values precludes a meaningful determination of a "best" value. However, the recent, precise $S(0)$ determinations (ours and Refs. [13–15]) all lie between 0.53 and 0.61keV b, suggesting that the true value of $S(0)$ also lies in this range. Comparing with older recommendations made before the recent measurements, this range is well inside the range recommended by NACRE [29], 0.54 ± 0.09 keV b, and somewhat higher than the ranges recommended by Ref. [12], 0.53 ± 0.05 keV b, and by Ref. [31], 0.51 ± 0.04 keV b.

Further progress will probably depend on new measurements. It may be important to note that a new measurement using a recoil separator to detect the ^{7}Be nuclei, previewed in Ref. [32], is in good agreement with the present results in the region of overlap near $E_{\text{c.m.}} = 1.2$ MeV.

VI. IMPACT ON SOLAR MODEL CALCULATIONS AND BIG BANG NUCLEOSYNTHESIS

Our value for $S(0)$ quoted above is 12% larger than the accepted value quoted in Ref. [12]. What would be the consequence of an upward adjustment of this size for solar model neutrino flux calculations and Big Bang Nucleosynthesis (BBN)?

It would increase the calculated Standard Solar Model (SSM) neutrino fluxes from decay of ^{7}Be and ^{8}B in the sun by approximately 10% [1]. Using old (new) heavy element abundances, Bahcall, Serenelli, and Basu [33] quote 1.09 (0.87) for the ratio of the calculated SSM to measured ^{8}B neutrino flux, where the measured flux has $\pm 9\%$ uncertainty [34] and the SSM flux has $\pm 16\%$ uncertainty (both 1σ). Thus a 10% upward adjustment of these calculated ^{8}B fluxes would not lead in either case to a significant disagreement with the measured flux, based on these uncertainties.

The uncertainty in the ^{3}He + ^{4}He $\rightarrow$ ^{7}Be $S(0)$ is one of the largest uncertainties that contribute to the SSM neutrino flux from ^{7}Be decay in the sun [1]; hence, an eventual reduction in this uncertainty will reduce significantly the uncertainty in the calculated SSM flux that the BOREXINO [35] and KamLAND [36] experiments are designed to observe.

The ^{7}Li problem in Big Bang Nucleosynthesis is well-known and long-standing: ^{7}Li, which results mainly from decay of ^{7}Be produced by the ^{3}He + ^{4}He $\rightarrow$ ^{7}Be reaction, is overpredicted by BBN calculations [2]. Thus an increase in the ^{3}He + ^{4}He $\rightarrow$ ^{7}Be reaction rate at BBN energies would worsen this discrepancy.

ACKNOWLEDGMENTS

We thank the CENPA technical staff, particularly G. C. Harper and D. I. Will for their support; R. Abel, M. K. Bacrania, A. M. Crisp, J. D. Lowrey, K. Michnicki, P. Peplowski, and J. Sibille for their help; P. D. Parker for helpful comments; and the U.S. DOE, Grant DE-FG02-97ER41020 for financial support.

[1] J. N. Bahcall and M. H. Pinsonneault, Phys. Rev. Lett. **92**, 121301 (2004).
[2] See, e.g., A. Coc, E. Vangioni-Flam, P. Descouvemont, A. Adahchour, and C. Angulo, Astrophys. J. **600**, 544 (2004).
[3] H. D. Holmgren and R. L. Johnston, Phys. Rev. **113**, 1556 (1959).
[4] P. D. Parker and R. W. Kavanagh, Phys. Rev. **131**, 2578 (1963); P. D. Parker, Ph.D. thesis, 1963; and (private commmunication, 2007).
[5] K. Nagatani, M. R. Dwarakanath, and D. Ashery, Nucl. Phys. **A128**, 325 (1969).
[6] H. Kräwinkel, H. W. Becker, L. Buchmann, J. Görres, K. U. Kettner, W. E. Kieser, R. Santo, P. Schmalbrock, H. P. Trautvetter, A. Vlieks, C. Rolfs, J. W. Hammer, R. E. Azuma, and W. S. Rodney, Z. Phys. A **304**, 307 (1982).
[7] J. L. Osborne, C. A. Barnes, R. W. Kavanagh, R. M. Kremer, G. J. Mathews, J. L. Zyskind, P. D. Parker, and A. J. Howard, Phys. Rev. Lett. **48**, 1664 (1982); J. Osborne, Ph.D. thesis, Caltech, 1983.
[8] T. K. Alexander, G. C. Ball, W. N. Lennard, H. Geissel, and H.-B. Mak, Nucl. Phys. **A427**, 526 (1984).
[9] M. Hilgemeier, H. W. Becker, C. Rolfs, H. P. Trautvetter, and J. W. Hammer, Z. Phys. A **329**, 243 (1988).
[10] R. G. H. Robertson, P. Dyer, T. J. Bowles, R. E. Brown, N. Jarmie, C. J. Maggiore, and S. M. Austin, Phys. Rev. C **27**, 11 (1983).

[11] H. Volk, H. Kräwinkel, R. Santoand, and L. Wallek, Z. Phys. A **310**, 91 (1983).
[12] E. G. Adelberger, S. M. Austin, J. N. Bahcall, A. B. Balantekin, G. Bogaert, L. S. Brown, L. Buchmannn, F. E. Cecil, A. E. Champagne, L. Braeckeleer, C. A. Duba, S. R. Elliot, S. J. Freedman, M. Gai, G. Goldring, C. R. Gould, A. Gruzinov, W. C. Haxton, K. M. Heeger, E. Henley, C. W. Johnson, M. Kamionkowski, R. W. Kavanagh, S. E. Koonin, K. Kubodera, K. Langanke, T. Motobayashi, V. Pandharipande, P. Parker, R. G. H. Robertson, C. Rolfs, R. F. Sawyer, N. Shaviv, T. D. Shoppa, K. A. Snover, E. Swanson, R. E. Tribble, S. Turck-Chiéze, and J. F. Wilkerson, Rev. Mod. Phys. **70**, 1265 (1998).
[13] B. S. Nara Singh, M. Hass, Y. Nir-El, and G. Haquin, Phys. Rev. Lett. **93**, 262503 (2004).
[14] D. Bemmerer, F. Confortola, H. Costantini, A. Formicola, G. Gyürky, R. Bonetti, C. Broggini, P. Corvisiero, Z. Elekes, Z. Fülöp, G. Gervino, A. Guglielmetti, C. Gustavino, G. Imbriani, M. Junker, M. Laubenstein, A. Lemut, B. Limata, V. Lozza, M. Marta, R. Menegazzo, P. Prati, V. Roca, C. Rolfs, C. Rossi Alvarez, E. Somorjai, O. Straniero, F. Strieder, F. Terrasi, and H. P. Trautvetter, Phys. Rev. Lett. **97**, 122502 (2006); Gy. Gyürky, F. Confortola, H. Costantini, A. Formicola, D. Bemmerer, R. Bonetti, C. Broggini, P. Corvisiero, Z. Elekes, Zs. Fülöp, G. Gervino, A. Guglielmetti, C. Gustavino, G. Imbriani, M. Junker, M. Laubenstein, A. Lemut, B. Limata, V. Lozza, M. Marta, R. Menegazzo, P. Prati, V. Roca, C. Rolfs, C. Rossi Alvarez, E. Somorjai, O. Straniero, F. Strieder, F. Terrasi, and H. P. Trautvetter, Phys. Rev. C **75**, 035805 (2007).
[15] F. Confortola, D. Bemmerer, H. Costantini, A. Formicola, Gy. Gyürky, P. Bezzon, R. Bonetti, C. Broggini, P. Corvisiero, Z. Elekes, Zs. Fülöp, G. Gervino, A. Guglielmetti, C. Gustavino, G. Imbriani, M. Junker, M. Laubenstein, A. Lemut, B. Limata, V. Lozza, M. Marta, R. Menegazzo, P. Prati, V. Roca, C. Rolfs, C. Rossi Alvarez, E. Somorjai, O. Straniero, F. Strieder, F. Terrasi, and H. P. Trautvetter, Phys. Rev. C **75**, 065803 (2007).
[16] Isotope Products Laboratory, Valencia, CA.
[17] F. Salvat, J. M. Fernandez-Varea, and J. Sempau, PENELOPE, OECD Nuclear Energy Agency Data Bank (http://www.nea.fr).
[18] J. F. Ziegler and J. P. Biersack, TRIM (2003-2.0), http://www.SRIM.org.
[19] D. R. Tilley, C. M. Cheves, J. L. Godwin, G. M. Hale, H. M. Hofmann, J. H. Kelley, C. G. Sheu, and H. R. Weller, Nucl. Phys. **A708**, 3 (2002), and http://www.tunl.duke.edu/nucldata/.
[20] Http://www.canberra.com/products/.
[21] M. Sataka, A. Yagishita, and Y. Nakai, J. Phys. B **23**, 1225 (1990).
[22] MKS Instruments, Wilmington, MA 01887.
[23] C. Bordeanu, J. Manor, P. N. Peplowski, K. A. Snover, and D. W. Storm, UW CENPA Annual Report 2003–2004, p. 33.
[24] T. A. Tombrello and P. D. Parker, Phys. Rev. **131**, 2582 (1963).
[25] B. T. Kim, T. Izumoto, and K. Nagatani, Phys. Rev. C **23**, 33 (1981).
[26] T. A. Tombrello and P. D. Parker, Phys. Rev. **130**, 1112 (1963); A. C. L. Barnard, C. M. Jones, and G. C. Phillips, Nucl. Phys. **50**, 629 (1964); R. J. Spiger and T. A. Tombrello, Phys. Rev. **163**, 964 (1967).
[27] G. Audi, A. H. Wapstra, and C. Thibault, Nucl. Phys. **A729**, 337 (2003).
[28] T. Kajino, H. Toki, and S. M. Austin, Astrophys. J. **319**, 531 (1987).
[29] C. Angulo, M. Arnould, M. Rayet, P. Descouvemont, D. Baye, C. Leclercq-Willain, A. Coc, S. Barhoumi, P. Aguer, C. Rolfs, R. Kunz, J. W. Hammer, A. Mayer, T. Paradellis, S. Kossionides, C. Chronidou, K. Spyrou, S. Degl'Innocenti, G. Fiorentini, B. Ricci, S. Zavatarelli, C. Providencia, H. Wolters, J. Soares, C. Grama, J. Rahighi, A. Shotter, and M. Lamehi Rachti, Nucl. Phys. **A656**, 3 (1999); http://pntpm.ulb.ac.be/Nacre/nacre.htm.
[30] K. A. Snover and A. E. Hurd, Phys. Rev. C **67**, 055801 (2003).
[31] P. Descouvemont, A. Adahchour, C. Angulo, A. Coc, and E. Vangioni-Flam, At. Data Nucl. Data Tables **88**, 203 (2004).
[32] F. Strieder and C. Rolfs, Prog. Part. Nucl. Phys. (in press).
[33] J. N. Bahcall, A. D. Serenelli, and S. Basu, Astrophys. J. **621**, L85 (2005).
[34] S. N. Ahmed, A. E. Anthony, E. W. Beier, A. Bellerive, S. D. Biller, J. Boger, M. G. Boulay, M. G. Bowler, T. J. Bowles, S. J. Brice, T. V. Bullard, Y. D. Chan, M. Chen, X. Chen, B. T. Cleveland, G. A. Cox, X. Dai, F. Dalnoki-Veress, P. J. Doe, R. S. Dosanjh, G. Doucas, M. R. Dragowsky, C. A. Duba, F. A. Duncan, M. Dunford, J. A. Dunmore, E. D. Earle, S. R. Elliott, H. C. Evans, G. T. Ewan, J. Farine, H. Fergani, F. Fleurot, J. A. Formaggio, M. M. Fowler, K. Frame, B. G. Fulsom, N. Gagnon, K. Graham, D. R. Grant, R. L. Hahn, J. C. Hall, A. L. Hallin, E. D. Hallman, A. S. Hamer, W. B. Handler, C. K. Hargrove, P. J. Harvey, R. Hazama, K. M. Heeger, W. J. Heintzelman, J. Heise, R. L. Helmer, R. J. Hemingway, A. Hime, M. A. Howe, P. Jagam, N. A. Jelley, J. R. Klein, M. S. Kos, A. V. Krumins, T. Kutter, C. C. M. Kyba, H. Labranche, R. Lange, J. Law, I. T. Lawson, K. T. Lesko, J. R. Leslie, I. Levine, S. Luoma, R. MacLellan, S. Majerus, H. B. Mak, J. Maneira, A. D. Marino, N. McCauley, A. B. McDonald, S. McGee, G. McGregor, C. Mifflin, K. K. S. Miknaitis, G. G. Miller, B. A. Moffat, C. W. Nally, B. G. Nickel, A. J. Noble, E. B. Norman, N. S. Oblath, C. E. Okada, R. W. Ollerhead, J. L. Orrell, S. M. Oser, C. Ouellet, S. J. M. Peeters, A. W. P. Poon, B. C. Robertson, R. G. H. Robertson, E. Rollin, S. S. E. Rosendahl, V. L. Rusu, M. H. Schwendener, O. Simard, J. J. Simpson, C. J. Sims, D. Sinclair, P. Skensved, M. W. E. Smith, N. Starinsky, R. G. Stokstad, L. C. Stonehill, R. Tafirout, Y. Takeuchi, G. Tesic, M. Thomson, M. Thorman, R. Van Berg, R. G. Van de Water, C. J. Virtue, B. L. Wall, D. Waller, C. E. Waltham, H. Wan Chan Tseung, D. L. Wark, N. West, J. B. Wilhelmy, J. F. Wilkerson, J. R. Wilson, J. M. Wouters, M. Yeh, and K. Zuber, Phys. Rev. Lett. **92**, 181301 (2004).
[35] C. Arpesella, G. Bellini, J. Benziger, S. Bonetti, B. Caccianiga, F. Calaprice, F. Dalnoki-Veress, D. D'Angelo, A. Etenko, H. de Kerret, A. Derbin, M. Deutsch, K. Fomenko, D. Franco, B. Freudiger, C. Galbiati, S. Gazzana, M. Giammarchi, M. Goeger-Neff, A. Goretti, C. Grieb, S. Hardy, Aldo Ianni, Andrea Ianni, M. Joyce, G. Korga, D. Kryn, M. Laubenstein, M. Leung, E. Litvinovich, P. Lombardi, L. Ludhova, I. Machulin, G. Manuzio, A. Martemianov, F. Masetti, K. McCarty, E. Meroni, L. Miramonti, M. Misiaszek, D. Montanari, M. E. Monzani, V. Muratova, L. Niedermeier, L. Oberauer, M. Obolensky, F. Ortica, M. Pallavicini, L. Papp, L. Perasso, R. S. Raghavan, G. Ranucci, A. Razeto, A. Sabelnikov, C. Salvo, S. Schönert, H. Simgen, O. Smirnov, M. Skorokhvatov, A. Sotnikov, S. Sukhotin, Y. Suvorov, V. Tarasenkov, R. Tartaglia, G. Testera, D. Vignaud, S. Vitale, R. B. Vogelaar, F. von Feilitzsch,

M. Wojcik, O. Zaimidoroga, S. Zavatarelli, and G. Zuzel, Astropart. Phys. (in press); www.arxiv.org, astro-ph: 0708.2251v1.

[36] K. Eguchi, S. Enomoto, K. Furuno, J. Goldman, H. Hanada, H. Ikeda, K. Ikeda, K. Inoue, K. Ishihara, W. Itoh, T. Iwamoto, T. Kawaguchi, T. Kawashima, H. Kinoshita, Y. Kishimoto, M. Koga, Y. Koseki, T. Maeda, T. Mitsui, M. Motoki, K. Nakajima, M. Nakajima, T. Nakajima, H. Ogawa, K. Owada, T. Sakabe, I. Shimizu, J. Shirai, F. Suekane, A. Suzuki, K. Tada, O. Tajima, T. Takayama, K. Tamae, H. Watanabe, J. Busenitz, Z. Djurcic, K. McKinny, D.-M. Mei, A. Piepke, E. Yakushev, B. E. Berger, Y. D. Chan, M. P. Decowski, D. A. Dwyer, S. J. Freedman, Y. Fu, B. K. Fujikawa, K. M. Heeger, K. T. Lesko, K.-B. Luk, H. Murayama, D. R. Nygren, C. E. Okada, A. W. P. Poon, H. M. Steiner, L. A. Winslow, G. A. Horton-Smith, R. D. McKeown, J. Ritter, B. Tipton, P. Vogel, C. E. Lane, T. Miletic, P. W. Gorham, G. Guillian, J. G. Learned, J. Maricic, S. Matsuno, S. Pakvasa, S. Dazeley, S. Hatakeyama, M. Murakami, R. C. Svoboda, B. D. Dieterle, M. DiMauro, J. Detwiler, G. Gratta, K. Ishii, N. Tolich, Y. Uchida, M. Batygov, W. Bugg, H. Cohn, Y. Efremenko, Y. Kamyshkov, A. Kozlov, Y. Nakamura, L. De Braeckeleer, C. R. Gould, H. J. Karwowski, D. M. Markoff, J. A. Messimore, K. Nakamura, R. M. Rohm, W. Tornow, A. R. Young, and Y.-F. Wang, Phys. Rev. Lett. **90**, 021802 (2003).